CRACK INITIATION MECHANISM OF BEARING STEEL IN VERY HIGH CYCLE FATIGUE

Tatsuo Sakai
College of Science and Engineering, Ritsumeikan University
1-1-1 Nojihigashi, Kusatsu, Shiga, 525-8577 Japan

Hisashi Harada and Noriyasu Oguma
R&D Center, Koyo Seiko Co., Ltd.
24-1 Kokubu Higanjyo-cho, Kashiwara, 582-8588 Japan

ABSTRACT

Mechanism of interior-inclusion induced fracture of bearing steel in long life region was experimentally examined under cantilever-type rotating bending. By means of FE-SEM, SIM and TEM, respectively, fracture surfaces and microstructures of the crack initiation sites were carefully observed. Thus, the fish-eye was usually found on the fracture surface in the interior-inclusion induced fracture, and an inclusion was always observed at the center of the fish-eye. Furthermore, a characteristic rough surface area was necessarily observed in the vicinity around the inclusion at the crack initiation site. Based on high-magnification FE-SEM observations at this characteristic area, it was found that morphology of this characteristic area became fine granular surface. This area was so-called "Fine Granular Area (FGA) in this paper. Based on TEM observation and X-ray diffraction pattern of the longitudinal section of the fracture surface at the FGA, the structural change was found around the inclusion to provide the microscopic polygonization along the FGA surface layer. Thickness of this fine granular layer is about 40nm, and some micro-debondings were observed along boundaries of this significant layer and matrix of the material. These facts suggest that the nucleation and coalescence of these micro-debondings provide the fatigue crack initiation process. Consequently, it is finally noted that the characteristic area of FGA is formed through the nucleation and coalescence of above micro-debondings.

Introduction

In the last decade, fatigue behavior of metallic materials in very high cycle regime has been coming out as an important subject to guarantee the safety of mechanical structures during the long term service[1-5]. The long term use of the mechanical structures provides us two typical advantages of saving the resources and reduction of the environmental load to the globe in the process of steel making[6]. Thus, the long term use of the mechanical structures can have a synergy effect of the reductions of resource consuming and environmental loads. As reported by many researchers[7-10], some of high strength steels and surface-hardened steels exhibit the significant fatigue property such that the *S-N* curve has a distinct knee point within a cycle range of $N=10^5$-10^6 and the curve has another knee point in the long life region of $N>10^7$. In other words, *S-N* curves of these steels tend to come down again in such a long life regime. This fact suggests that the endurance limit in the conventional concept cannot provide the safety design data for mechanical structures[11].

Fatigue tests in the long life regime take a long time and this is a typical difficulty to facilitate the research in the long life fatigue of metallic materials. In order to overcome this difficulty, the authors had developed special fatigue testing machines to perform the fatigue tests effectively in both rotating bending and axial loading in gigacycle regime[1,12]. By using these testing machines, one can perform fatigue tests for four specimens simultaneously. Thus, long life fatigue tests were carried out for several kinds of metallic materials including the high carbon chromium bearing steel(JIS:SUJ2) as a part of the round-robin tests in the Research Group for Statistical Aspects of Materials Strength(RGSAMS)[13].

In this paper, the fatigue property of SUJ2 steel in the gigacycle regime was first examined in the type of rotating bending and the duplex *S-N* characteristics consisting of the respective *S-N* curves for the surface induced fracture and the interior-inclusion induced fracture were again confirmed. Since main target of this study is the crack initiation mechanism in the long life regime, fracture surfaces of the latter fracture mode were carefully observed by FE-SEM paying an attention to the crack initiation site. Thus, fish-eye was always observed on the fracture surface in the latter fracture mode and an inclusion was necessarily found at the center of the fish-eye. In addition, in the vicinity around the inclusion, a characteristic area having the distinct fine granular morphology was always observed and this area was so-called "Fine Granular Area(FGA)". In order to analyze the crack initiation mechanism, microstructure of the FGA was directly observed by means of TEM and the X-ray diffraction pattern was also analyzed for the surface layer of the FGA. Based on these observations, the crack initiation mechanism in the very high cycle fatigue was discussed.

Specimens and Experimental Procedure

The material used in this study is a high carbon chromium steel for the bearing use(JIS:SUJ2). Chemical composition of this steel is shown in Table 1. Specimens were machined into the shape and dimensions as shown in Figure 1. Heat treatment conditions of the material were indicated as follows;

Quenched: 835deg.C x 40min + Oil quenching and Tempered: 180deg.C x 120min + Air cooling

Table 1. Chemical composition (mass%)

C	Si	Mn	Cr	Ti	[O]
0.98	0.24	0.3	1.44	0.0021	9ppm

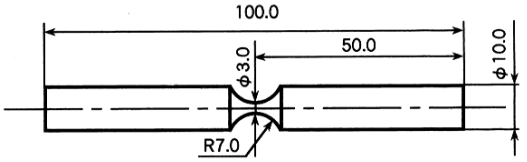

Stress concentration factor $\alpha = 1.06$

Figure 1 Shape and dimensions of specimen

Fatigue tests in rotating bending were performed in the ordinary room atmosphere without control of the temperature and the humidity by means of a dual-spindle testing machine as shown in Figure 2. This machine was originally developed by the authors in order to perform fatigue tests in very high cycle regime within the reasonable testing period. Fatigue tests of four specimens can be performed simultaneously by this machine. The rotating speed of the specimen was 3150rpm. The detailed structure and the performance were indicated in their earlier works[1,10].

Figure 2. Dual-spindle fatigue testing machine in rotating bending

Experimental Results of *S-N* Characteristics

Fatigue test data of SUJ2 steel obtained in the gigacycle regime were plotted as an *S-N* diagram in Figure 3. Fatigue tests were conducted for specimens prepared from two different lots of the same steel. The fracture surface of every failed specimen was observed by FE-SEM in order to distinguish the fracture modes of the surface induced fracture and the

interior-inclusion induced fracture. Open marks in Figure 3 indicate the results in the surface induced fracture, whereas solid marks the results in the interior-inclusion induced fracture. A clear knee point was found at N=10^5 in the *S-N* curve for the former fracture mode, but we have another *S-N* curve for the latter fracture mode. Thus, it was found that the complicated fatigue property of this steel can be well interpreted as the "Duplex *S-N* characteristics" consisting of the respective fracture modes. This aspect in the rotating bending fatigue tests was repeatedly confirmed by many researchers[1,10,14-16]. However, existence of the fatigue limit in the interior-inclusion induced fracture was not confirmed yet, even if fatigue tests were carried out toward the gigacycle regime.

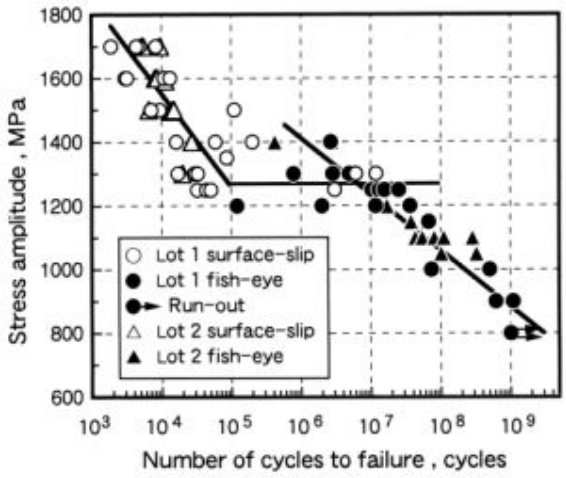

Figure 3. *S-N* diagram of SUJ2 steel.

Microscopic Observations of Fracture Surfaces

Figure 4 shows an example of Field Emission Scanning Electron Microscope(FE-SEM) images at the center of a fish-eye on a fracture surface of specimen failed in the interior-inclusion induced fracture($\sigma_a = 1100$ MPa, N=2.85x10^8). A non-metallic inclusion was observed at the center of the fish-eye. This non-metallic inclusion was analyzed to be TiN. The Fine Granular Area(FGA) was clearly observed around the inclusion. Thus, the fracture surface in the FGA has a distinct roughness as reported in the authors' earlier papers[1,6,10,12] and some papers by other researchers[14,16]. Figure 4(b) indicates the high magnification image of the area enclosed by the white square frame in Figure 4(a). In

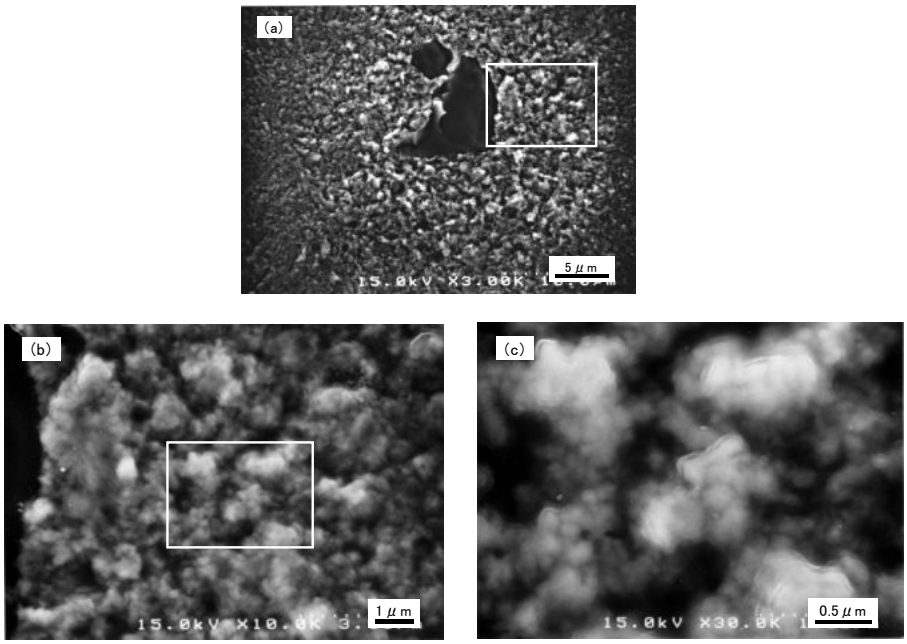

Figure 4. FE-SEM images in the vicinity around non-metallic inclusion

addition, an area enclosed by the white square frame in Figure 4(b) was again observed in the higher magnification and the image was indicated in Figure 4(c). One can well trace the morphology of the fracture surface in each image in Figure 4(a), (b) and (c), respectively.

Fracture surface of the opposite side of the same failed specimen was similarly observed by FE-SEM. Thus, we found that the white portion inside the FE-SEM image is beautifully corresponding to the dark portion of the opposite fracture surface. By performing such matching observations for a pair of fracture surfaces, it was found that a concave portion of a fracture surface well corresponds to the convex portion of the opposite fracture surface of the same specimen. This fact suggests that the separation of microscopic curved boundaries is more instructive rather than the formation of micro-voids, since such voids have to produce concave morphology at both sides of the fracture surface.

In FE-SEM observations of the fracture surface, the authors had noticed an interesting aspect that a distinct difference was found in the images observed in the different acceleration voltages. Figure 5 shows the FE-SEM images of the FGA thus observed by different voltages. Figure 5(a) indicates the result observed at 5kV of the acceleration voltage, whereas Figure 5(b) the result obtained at the different voltage of 30kV. In the case of 5kV, the electron penetrating depth is shallow comparing with the corresponding depth at the voltage of 30kV. From this point of view, FE-SEM image at the higher voltage provides an image reflecting the microstructure of the surface layer having a sufficient thickness, but the image at the lower voltage provides the corresponding image reflecting the microstructure of only very thin surface layer. If the microstructures in the very shallow surface layer and a little deep layer are the quite same, both FE-SEM images would come close to each other. However, if the microstructures of the shallow surface layer and the deep layer have a distinct difference, FE-SEM images obtained by different acceleration voltages should be reflected distinctly. In other words, if a distinct difference was found between two FE-SEM images taken at different voltages, then a marked difference would be caused in the microstructure in each layer. This fact suggests that the microstructure of very shallow layer is distinctly differ from that of a little deep layer. As mentioned above, the fine granular morphology can be observed around the inclusion on the fracture surface, but such a characteristic morphology cannot be found in the other area. Accordingly, it should be noted that the extensive polygonization can take place within only very shallow surface layer inside the FGA.

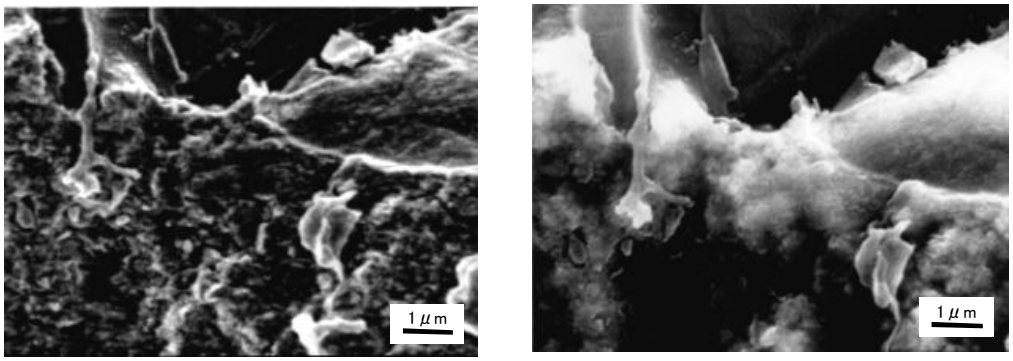

(a) Acceleration voltage : 5kV (b) Acceleration voltage : 30kV

Figure 5. FE-SEM images of FGA observed at different acceleration voltage.

Microscopic Observations of Cross Section of FGA

Figure 6 indicates an example of FE-SEM image around a non-metallic inclusion at the crack initiation site of a specimen failed at $\sigma_a = 900$ MPa and N=1.08x10^9. A clear area of FGA surrounded by a dotted circle was observed and the morphology inside the FGA is quite similar to that in Figure 4(a). This feature inside the FGA is very common in the crack initiation site for every specimen failed in the interior-inclusion induced fracture mode. In order to examine a microstructural change of the surface layer of the FGA, the longitudinal section of the fracture surface was observed by means of a scanning ion microscope(SIM). The longitudinal section of the FGA was carefully produced by gallium ion sputtering technique using a focused ion beam system(FIB).

At first, the longitudinal section at the position of (1) inside the FGA in Figure 6 was observed by SIM, and the result was shown in Figure 7(a). Another position (2) outside the FGA was also observed by the same technique and the photograph was given in Figure 7(b). The top edge of each image provides the fracture surface of position (1) or (2) in Figure 6. Comparing these two photographs with each other, one can find that the microstructure in a thin surface layer of the fracture surface in Figure 7(a) becomes fine granular, but such a fine granular region was not observed in the microstructure in Figure 7(b) corresponding to the position of (2) outside the FGA. Paying a particular attention to the top edge of the section in Figure 7(a), the fine granular area was not spread throughout the FGA surface. The fine granular layer is observed in the limited area in the fracture surface inside the FGA. This fact suggests that the some parts of the fine granular layer are adjoining with the fracture surface of the present half specimen and other parts of the fine granular

layer are remaining at the fracture surface of the opposite half specimen. In other words, the fine granular layer is induced around a non-metallic inclusion inside the material during the long-term sequence of stress cycles and a pair of boundaries between matrix and this thin layer tend to debond depending on the boundary strength. If the debonding occurs at the top boundary of the fine granular layer, the thin layer is kept on the bottom specimen, but the layer is kept on the top specimen when the debonding takes place at the bottom boundary. In this manner, some parts of the fine granular layer are remaining on the top specimen, while some other parts of the layer are on the bottom specimen. However, such a phenomenon is not observed outside the FGA, since the fine granular layer is no longer induced in this area.

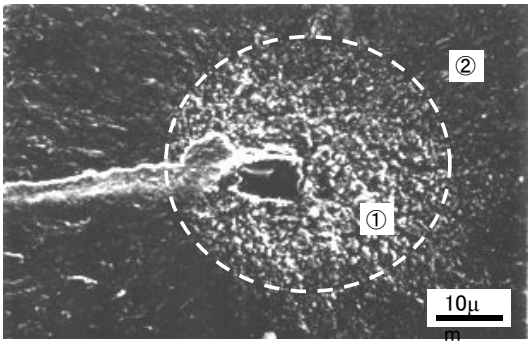

Figure 6. An example of FE-SEM image of FGA on fracture surface.

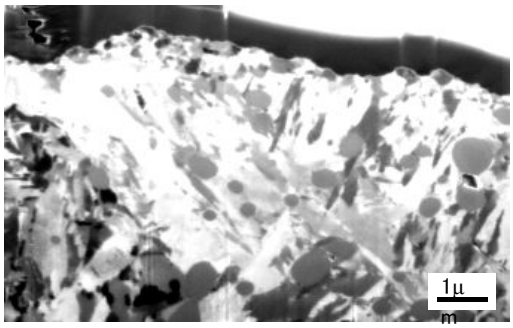

(a) Inside FGA : part① in Figure

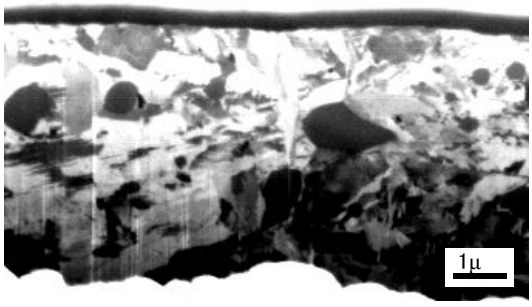

(b) Outside FGA : part② in Figure

Figure 7. SIM image of longitudinal section of fracture

The microstructure inside the fine granular area(FGA) in Figure 7(a) was again observed by a transmission electron microscope(TEM). The TEM specimen was prepared by means of a special technique of Focused Ion Beam System(FIB), and thickness of this specimen was 30nm, approximately. A bright field image of TEM observation thus obtained is given in Figure 8. The mark of A indicates the fine granular layer inside FGA, whereas the other mark of B is indicated at the deep position where the fine polygonization was not observed. X-ray diffraction patterns at areas A and B in Figure 8 are indicated in Figure 9(a) and (b), respectively. The diffraction pattern at area of A in Figure 8 gives a ring-like pattern, while

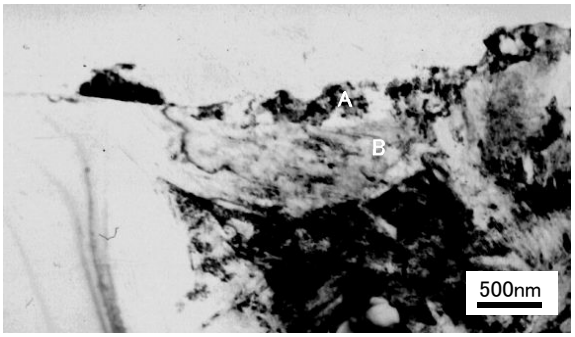

Figure 8. TEM image of longitudinal section of FGA in bright field

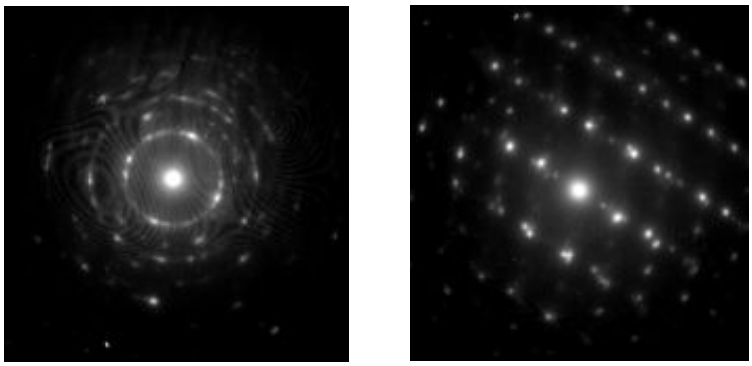

(a) Part A (b) Part B

Figure 9. Selected area X-ray diffraction patterns in thin layer and deep position.

the corresponding image at area of B in Figure 8 provides the spot-like pattern peculiar to the martensitic structure of this steel.

The ring-like pattern in Figure 9(a) is given when a number of subgrains are participating in the diffraction at very limited area, whereas the spot-like pattern in Figure 9(b) is obtained from a definite crystal depending on the crystal structure. From this point of view, one can conclude that a lot of fine subgrains having different crystal orientations are produced within the thin layer around the non-metallic inclusion during a number of stress cycles. Thickness of this fine granular layer having the characteristic feature is within 400nm as seen in Figure 8. This value is well corresponding to the thickness of the fine granular layer to be observed in Figure 7(a).

Mechanism of Crack Initiation in Very High Cycle Fatigue

As shown in the previous section, the authors have observed the microstructure inside the fine granular area(FGA) for several specimens by using the same procedure, and common results are obtained for every observation. Thus, the characteristic area of FGA around the non-metallic inclusion at the crack initiation site is a common feature in the very high cycle fatigue. Based on the microscopic observations by FE-SEM and SIM together with the analysis of X-ray diffraction patterns of the microstructure, mechanism of the fatigue crack initiation in the very high cycle regime would be assumed to have following four stages as illustrated in Figure 10.

Stage A : a fine granular layer caused by the intensive polygonization is gradually induced around the interior-inclusion during a long sequence of the cyclic loading. [Formation of fine granular layer]
Stage B : microscopic debondings take place along the boundaries between the fine granular layer and the matrix of the material depending on the strength level at each site of the boundaryies. [Nucleation of micro-debondings]
Stage C : number of micro-debondings is increased gradually and some of them would coalesce to one another. [Nucleation and coalescence of micro-debondings]
Stage D : micro-debondings are entirely spread over the fine granular layer and the penny-shape crack is finally formed around the interior-inclusion of the material. [Completed formation of the fine granular area(FGA)]

In Figure 10, the longitudinal sections passing through the inclusion at the crack initiation site are indicated in the left hand side, while the cross sections passing through the same inclusion are given in the right hand side, respectively. Some segments of thick solid lines in the left hand side indicate the micro-debondings along the boundaries between the fine granular layer and the matrix of the material. Thickness of the fine granular layer is within 400nm. At the final stage(Stage D), all the segmentations are adjoined to one another by penetrating the fine granular layer so that a rough surface area is produced as the fine granular area(FGA). White spots in the illustrations of the right hand side indicate micro-debondings along the top boundary, whereas black spots provide the micro-debondings along the bottom boundary. Thus, all of these white and black spots are adjoined at the final stage of the crack initiation(Stage D), and the penny-shape crack is produced around the inclusion. Based on this mechanism, the significant morphology to have the distinct rough surface is produced inside the FGA. In this manner, the characteristic area of FGA is produced in the long sequence of the cyclic loadings in the very high cycle fatigue. As reported in the earlier works[17,18], once the crack size exceeds the critical size giving the threshold value for the fatigue crack propagation at the FGA front, the fatigue crack tends to grow by each cycle of the applied load as governed by the Paris' law of the fatigue crack propagation[19],

Stress intensity factor range ΔK at the FGA front takes values within 4-6MPa$\sqrt{m}$ regardless of the level of the applied stress and the inclusion size. This value is well corresponding to the threshold value of the fatigue crack propagation as reported by many researchers[17,20,21]. This fact suggests that the fatigue behavior inside the FGA does not correspond

to the crack propagation. This process should be interpreted as a crack initiation process instead of the crack propagation. According to experimental works by Y. Kuroshima[22], K. Shiozawa[21] and M. Nakajima[23], micro-debondings take place isolatedly inside the FGA and these micro-debondings adjoin altogether at a certain stage of cyclic loadings. These results can provide an experimental evidence to assume that the fatigue process inside the FGA is corresponding to the crack initiation instead of the crack propagation. However, some other mechanisms of the fatigue crack initiation were also proposed by several researchers[21,22,24], and the mechanism would depend on the kind of material and the testing conditions. In order to clarify the mechanism, further experimental evidences should be accumulated for various kinds of metallic materials in the future.

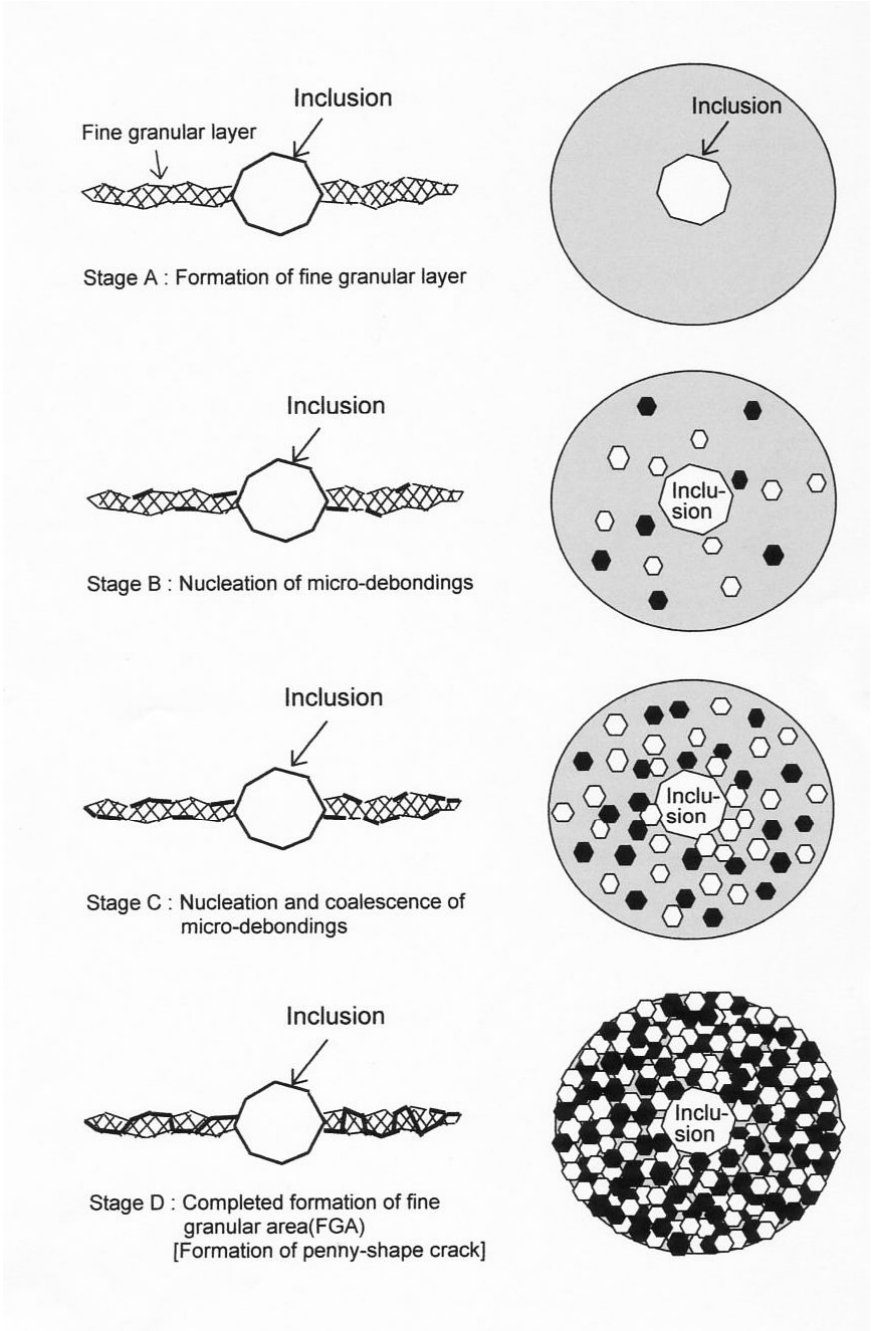

Figure 10 Illustration of fatigue crack initiation process in the interior-inclusion induced fracture in very high cycle fatigue

Conclusions

Fatigue property of a high carbon chromium bearing steel(SUJ2) in very high cycle regime was experimentally examined and the crack initiation mechanism was discussed. Main conclusions obtained in this work are summarized as follows;

(1) Significant duplex *S-N* curves consisting of those for the surface induced fracture and the interior-inclusion induced

fracture were reconfirmed in rotating bending. In the latter fracture mode, a fish-eye was necessarily observed on the fracture surface and a non-metallic inclusion was usually found at the center of the fish-eye.

(2) Characteristic area of fine granular area(FGA) was necessarily formed around the inclusion at the crack initiation site. By performing some matching observations for a pair of fracture surfaces, debondings of microscopic curved boundaries in the FGA was caused as the crack nucleation process instead of the formation of micro-voids.

(3) Based on FE-SEM and TEM observations together with X-ray diffraction analysis, it was found that the fatigue crack in very high cycle fatigue was caused through the following mechanisms; Stage A(Formation of fine granular layer around an inclusion), Stage B(Nucleation of micro-debondings), Stage C(Nucleation and coalescence of micro-debondings) and Stage D(Formation of penny-shape crack).

References

1. Sakai, T., Takeda, M., Shiozawa, K., Ochi, Y., Nakajima, M., Nakamura, T. and Oguma, N., "Experimental reconfirmation of characteristic S-N property for high carbon chromium bearing steel in wide life region in rotating bending", *J. Soc. Mat. Sci., Japan*, **49**, 779-785, (2000).
2. Bathias, C., "Relation between endurance limits and thresholds in the field of gigacycle fatigue", *ASTM STP* 1372, 135-154, (2000).
3. Stanzl-Tschegg, S E., "Fracture mechanisms and fracture mechanics at ultrasonic frequencies", *Fatigue Fract Eng Mater Struct,* **22**, 567-579, (1999).
4. Mayer, H., "Fatigue lifetime investigations in the very high cycle regime using the ultrasonic resonance testing method", *Proc. VHCF-3*, 448-455, (2004).
5. Zhu, X., Shyam, A., Jones, J. W., Mayer, H., Lasecki, J. V. and Allison, J. E., "Elevated temperature fatigue behavior of a 319 cast aluminum alloy in the gigacycle regime", *Proc. VHCF-3*, 448-455, (2004).
6. Sakai, T., Takizawa, R., Furusawa, T., Nakajima, M., Shiozawa, K. and Oguma, N., "Reliability evaluation of SUJ2 in long life regime by the multi-type axial fatigue testing machine", *Proc. EcoDesign2005*, CD-ROM, (2005).
7. Naito, T., Ueda, H. and Kikuchi, M., "Fatigue behavior of carburized steel with internal oxides and nonmartensitic microstructure near the surface", *Metal. Trans*., **15A**, 1431-1436, (1984).
8. Asami, K. and Sugiyama, Y., "Fatigue strength of various surface hardened steels", *J. Heat Treatment Technol. Assoc*., 25, 147-150, (1985).
9. Ochi, Y, Sakai, T., "Fatigue of metallic materials in the very high cycle regime", *J. Soc. Mat. Sci. Japan*, **52**, 433-439, (2003).
10. Sakai, T., Takeda, M., Shiozawa, K., Ochi, Y., Nakajima, M., Nakamura, T. and Oguma, N., "Experimental evidence of duplex S-N characteristics in wide life region for high strength steels", *Proc. 7th Int. Fat. Congr. FATIGUE'99*, Vol.**1**, 573-578, (1999).
11. Sakai, T., "Fatigue characteristics of metallic materials –Mainly focusing to bearing steels–", *Inspection Engineering*, **9**, 1-7, (2004).
12. Sakai, T., Furusawa, T., Takizawa, R., Nakajima, M., Shiozawa, K., Oguma, N., Okada, K., Ochi, Y., Sugeta, A., Kawagoishi, N., Sakaida, A. and Sakamoto, H., "Development of multi-type fatigue testing machine in axial loading and some fatigue test results on a bearing steel", *Proc. VHCF-3*, 484-491, (2004).
13. Nishikawa, I., Sugeta, A., Sakai, T., Shuto, T., Yoshida, T. and Inoue, A., "Material strength database for reliability design of machines and structures combined with a software of STANAD", *Proc. 5th Japan International SAMPE Symposium*, 289-294, (1997).
14. Shiozawa, K. Lu, L. T. and Ishihara, S., "Subsurface fatigue crack initiation behavior and S-N curve characteristics in high carbon chromium bearing steel", *J. Soc. Mat. Sci., Japan*, **48**, 1095-1100, (1999).
15. Goto, M., Yamamoto, T., Nisitani, H., Sakai, T. and Kawagoishi, N., "Effect of grinding on the fatigue strength of a bearing steel in the super long-life field", *Proc. ECF-13*, CD-Rom(Paper reference: 3C.167), (2000).
16. Nakajima, M., Sakai, T. and Shimizu, T., "An observation of fish-eye fracture process in high strength steel SUJ2", *Trans. Jpn. Soc. Mech. Eng*, **A-65**, 2504-2510, (1999).
17. Sakai T., Sato, Y. and Oguma, N., "Characteristic *S-N* property of high carbon chromium bearing steel under axial loading in long life fatigue", *Fatigue Fract Eng Mater Struct*, **25**, 765-773, (2002).
18. Sakai, T., Sato, Y., Nagano, Y., Takeda, M. and Oguma N., "Effect of stress ratio on long life fatigue behavior of high carbon chromium bearing steel under axial loading", *Proc. VHCF-3*, 209-216, (2004).
19. Paris, P. C. and Erdogan, F., "A critical analysis of crack propagation laws", *Trans. ASME,* Ser.D, **85**-4, 528-534, (1963).
20. Beswick, J. M., "Fracture and fatigue crack propagation properties of hardened 52100 steel", *Metal. Trans*., **20**A, 1961-1973, (1989).
21. Shiozawa, K., Morii, Y., Nishino, S. and Lu, L., "A study of subsurface crack initiation and propagation mechanism of high-strength steel by fracture surface topographic analysis", *J. Soc. Mat. Sci., Japan*, **52**, 1311-1317, (1999).
22. Kuroshima, Y., Ikeda, T., Harada, M. and Harada, S.,"Subsurface crack growth behavior on high cycle fatigue of high strength steel", *Trans. Jpn. Soc. Mech. Eng.*, **A-64**, 2536-2541, (1998).
23. Nakajima, M., Kamiya, N., Itoga, H., Tokaji, K. and Ko, H-N., "Experimental estimation of subsurface crack initiation lives and Intrinsic fatigue limit in a high strength steel", *Trans. Jpn. Soc. Mech. Eng*., **A-70**, 1636-1642, (2004).
24. Murakami, Y., Nomoto, T., Ueda, T., Murakami, Y. and Ohori, M., "Analysis of the mechanism of superlong fatigue failure by optical microscope and SEM/AFM observations", *J. Soc. Mat. Sci., Japan*, **48**, 1112-1117, (1999).